Electronic structures and abnormal phonon behaviors of cobalt-modified Na0.5Bi0.5TiO3-6%BaTiO3 single crystals

T. Huang, P. Zhang, L. P. Xu, C. Chen, J. Z. Zhang, Z. G. Hu, H. S. Luo, and J. H. Chu

Citation: AIP Advances **6**, 105311 (2016); doi: 10.1063/1.4966910
View online: http://dx.doi.org/10.1063/1.4966910
View Table of Contents: http://scitation.aip.org/content/aip/journal/adva/6/10?ver=pdfcov
Published by the AIP Publishing

Electronic structures and abnormal phonon behaviors of cobalt-modified $Na_{0.5}Bi_{0.5}TiO_3$-6%$BaTiO_3$ single crystals

T. Huang,[1] P. Zhang,[1] L. P. Xu,[1] C. Chen,[2] J. Z. Zhang,[1] Z. G. Hu (胡志高),[1,a] H. S. Luo,[3] and J. H. Chu[1]

[1]*Technical Center for Multifunctional Magneto-Optical Spectroscopy (ECNU), Shanghai, China and Department of Electronic Engineering, East China Normal University, Shanghai 200241, China*

[2]*Jiangxi Key Laboratory of Advanced Ceramic Materials, Department of Materials Science and Engineering, Jingdezhen Ceramic Institute, Jingdezhen 333001, China*

[3]*R&D Center of Synthetic Crystals, Shanghai Institute of Ceramics, Chinese Academy of Sciences, Shanghai 201800, China*

(Received 10 June 2016; accepted 20 October 2016; published online 27 October 2016)

Optical properties, electronic structures, and structural variations of x wt% cobalt (Co) doped $Na_{0.5}Bi_{0.5}TiO_3$-6%$BaTiO_3$ (x=0%, 0.5%, 0.8%) single crystals have been studied by temperature-dependent optical ellipsometry and Raman spectra from 250 to 650 K. Based on the temperature evolution of electronic transitions (E_{cp1} and E_{cp2}) and the phonon modes involving Ti-O vibrations, two critical temperature points exhibit an increasing trend with Co dopants, which are related to structural variations for ferroelectric to anti-ferroelectric, and anti-ferroelectric to paraelectric transition, respectively. Additionally, distinguishing abnormal phonon behaviors can be observed from Raman spectra for the crystal of x=0.5% and 0.8%, which show reverse frequency shift of the modes involving Ti-O vibration. It can be ascribed to different relative concentration of Co^{2+} and Co^{3+} in the crystals, which has been confirmed by X-ray Photoelectron Spectroscopy data. [http://dx.doi.org/10.1063/1.4966910]

I. INTRODUCTION

In recent years, lead-free ferroelectrics have attracted considerable attentions for the outstanding advantages in free control of sintering atmosphere and lacking of lead pollution during the process of preparation. In this regard, $Na_{0.5}Bi_{0.5}TiO_3$-based perovskites, which exhibit relatively large spontaneous polarization and high Curie temperature, are leading candidate that have been widely studied.[1–5] Among these, the $Na_{0.5}Bi_{0.5}TiO_3$-x%$BaTiO_3$ (NBBTx%) binary system possess a rhombohedral-tetragonal morphotropic phase boundary in the region of $6<x<8$,[1] where the system provides remarkably superior piezoelectric and dielectric properties than other NBT-based lead-free materials.[1,3]

To meet the stringent requirements for specific applications, however, the electrical properties of the NBBTx% compositions need to be optimized,[6] which can be overcome through compositional modification by oxide doping. For example, cobalt oxide is believed to be an effective additive, based on the researches about Pb-, $K_{0.5}N_{0.5}NbO_3$- and $Na_{0.5}Bi_{0.5}TiO_3$-based ceramics, even adding a small amount of dopants.[6–11] To further understand the doping mechanism of Co cations, it's significant to take the valence state of Co cations in the ceramics/crystals into account.[8,9] In most of the studies, Co cations are thought to exist only in Co^{2+} or Co^{3+} state.[6,7] Moreover, It has been demonstrated

[a]Author to whom correspondence should be addressed. Tel.: +86-21-54345150. Fax: +86-21-54345119. Electronic mail: zghu@ee.ecnu.edu.cn

that both Co^{2+} and Co^{3+} cations coexist in Co doped ceramics, and their relative concentrations are strongly associated with the addition.[8,9]

Furthermore, optical spectra have been proven to be a powerful approach to investigate related issues on local configurations and phase transition.[12–15] Optical ellipsometry, has been considered as a novel and powerful technique to investigate the thickness and complex dielectric function ($\varepsilon=\varepsilon_1+i\varepsilon_2$) of a studied system. Besides, interband critical points (CPs), obtained from optical ellipsometry data, have shown efficiency in exploring phase transition of ferroelectrics.[12,13] Similarly, as a nondestructive characterization technique, Raman scattering is sensitive to symmetry disturbance and can provide precise information about ionic configurations and local distortions in materials,[15] which has been applied as a crucial tool for investigating phase transition in ferroelectrics.[4,14,15] Based on the spectral analysis, the phonon modes can be explained by the variations of frequency, intensity, and full width at half maximum (FWHM).

In this work, the electronic transitions and phonon modes of x wt% Co doped $Na_{0.5}Bi_{0.5}TiO_3$-6%$BaTiO_3$ (x%-Co:NBBT6, x=0%, 0.5% and 0.8%) single crystals have been investigated by optical ellipsometry and Raman spectra as a function of temperature from 250 to 650 K, respectively. Remarkably, distinguishing abnormal phonon behaviors of x=0.5% and 0.8% are observed from Raman spectra. It can be associated with different relative concentration of Co^{2+} and Co^{3+} in the crystals, which was confirmed by X-ray Photoelectron Spectroscopy data. The physical mechanism has also been discussed in detail.

II. EXPERIMENTAL DETAILS

Single crystals of x%-Co:NBBT6 (x=0%, 0.5% and 0.8% in melting) were grown using the top-seeded solution growth technique.[3] The obtained specimens were cut into the size about $10\times10\times0.4$ mm^3, parallel the $(001)_{PC}$ face with single-side polished. Before spectral measurements, the specimens have been annealed (~400 °C) after the mechanical polishing, then cleaned in pure ethanol with an ultrasonic bath and rinsed by deionized water for several times. The root-mean-square roughness of the crystals were estimated to be about 5 nm by atomic force microscopy (AFM, Digital Instruments Dimension Icon, Bruker). Optical ellipsometry experiments were performed by optical ellipsometry (J.A. Woollam Co., Inc.) in the range of 2-6 eV with an incident angle of 70°. The spectral resolution of optical ellipsometry is set to 5 nm, and the measurements were carried out with auto retarder (high accuracy). Note that all the fitting procedure was completed through WVASE32 software package. Raman scattering measurements were carried out by a Jobin-Yvon LabRAM HR 800 micro-Raman spectrometer and a THMSE 600 heating/cooling stage (Linkam Scientific Instruments), with 632.8 nm laser used as the excitation source. The spectral resolution of Raman spectra is better than 0.65 cm^{-1}, and an air-cooled charge coupled device was used to collect the scattered signal dispersed on 1800 grooves/mm grating in the frequency range of 10-950 cm^{-1}, with the use of ultra low frequency filter.[12] For both ellipsometric and Raman experiments, the temperature was varied from 250 to 650 K at addition of 25 K, with resolution of 0.1 K. The valence state of Co cations in single crystals were investigated by X-ray photoelectron spectroscopy experiments on a RBD upgraded PHI-5000C ESCA system (Perkin-Elmer) with Mg $K\alpha$ radiation (hv =1253.6 eV).

III. RESULTS AND DISCUSSION

Fig. 1(a) depicts the real part ε_1 and imaginary part ε_2 of numerically inverted complex dielectric function (NICDF) for x%-Co:NBBT6 single crystals at three different temperatures, respectively, which were directly calculated from the original experimental data with the accurate thickness of the roughness layer.[12,13] As can be seen, the NICDF of x%-Co:NBBT6 crystals showing the similar trend. Firstly, the ε_2 of all specimens is near to zero except when the photon energy increased close to the band gap energy (~3 ev), then exhibits obvious dispersion with increasing photon energy, due to the electronic transition. Furthermore, ε_2 generally exhibits a red shift on heating, which can be attributed to electron-phonon interaction and the lattice thermal expansion.[12] As for x%-Co:NBBT6 crystal, the BO_6 octahedron governs the lower-lying conduction bands and the upper

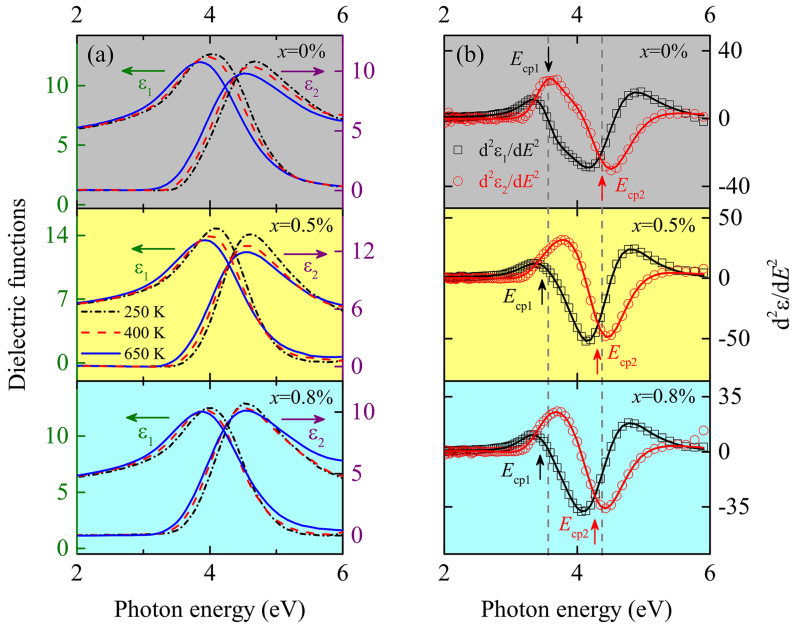

FIG. 1. (a) The real part ε_1 (using the left vertical axis) and imaginary part ε_2 (corresponding to the right vertical axis) of numerically inverted complex dielectric function (NICDF) of x%-Co:NBBT6 (x=0%, 0.5%, and 0.8%) single crystals, measured at 250, 400, and 650 K. (b) The second derivative of NICDF (dots) and the best-fit curves (lines) for samples at 300 K. Note that, the critical-point positions (E_{cp1} and E_{cp2}) are marked with arrows in each section, according to the best-fitting parameters of SCP model from Table I. The dash line was applied to distinguish the positions.

valence bands. In other words, the B-site *d* orbitals and the O-anion 2*p* orbitals associated with each octahedron are the major contributors to the energy bands.[16] Other ions in the structure contribute to the higher-lying conduction states, which are of negligible importance provided the electronic polarizability, and have only a small effect on optical properties.[17] Accordingly, x%-Co:NBBT6 single crystals have similar optical absorption edges with slight differences due to different B-site (Co, Ti) cations.

The second derivative of the NICDF was fitted with the standard critical point (SCP) model to obtain the accurate energies E_{cp} and determine the temperature dependence of CP structures. Note that, the detailed process of obtaining the value of E_{cp} has been described in the previous works, please refer to Refs. 12 and 13. For clarity, the set of the fitting parameters is listed in Table I. In this work, the parameter n was set to -1, which is consistent with the value for previously reported NBBT6 single crystals.[12] Fig. 1(b) presents the second derivatives spectra of the NICDF, as well as the best-fitting curves at 300 K for x=0%, 0.5%, and 0.8%, respectively. As can be discerned, two distinct transitions can be readily distinguished. Based on the fitting parameters at 300 K from Table I, the value of first CP (E_{cp1}) for x=0%, 0.5%, and 0.8% is 3.56, 3.47, and 3.44 eV, respectively, mainly determined by the transitions from the O-2*p* VB to Ti-3*d* or Bi-6*p* lower-energy CB; the value of second one (E_{cp2}) is 4.37, 4.30, and 4.26 eV, respectively, corresponding to the transition from O-2*p* VB to Ti-3*d* or Bi-6*p* high-energy CB.[16] It indicates that the band gaps of x%-Co:NBBT6 crystals decrease with increasing Co dopants. This observation could be explained by the *sp-d* exchange interactions between the band electrons and localized *d* electrons of Co ions substituting Ti^{4+} ions. The *s-d* and *p-d* exchange interactions can give rise to the decline of the conduction band bottom, leading to the band gap narrowing.[18]

Fig. 2(a) and (b) plot the temperature dependence of E_{cp1} and E_{cp2} energy for all crystals, respectively. Note that, all the fitting parameters, including the ones at 300 K, is listed in Table I. The consistency of the phase angle value (ϕ_m) for all temperatures confirms the excitonic metamorphism of the second derivative of NICDF (presented by n=−1) and the robustness of the fitting procedure.[13] As can be observed, all of the E_{cp1} and E_{cp2} energies generally show a red shift trend with increasing the temperature, which are consistent with the above observation about ε_2 from Fig. 1(a). Moreover,

Table I. The best-fitting parameters of SCP model for x%-Co:NBBT6 (x=0%, 0.5% and 0.8%) single crystals extracted from the second derivative of NICDF at specific temperatures.

	$x = 0\%$					$x = 0.5\%$					$x = 0.8\%$				
Temperature (K)	250	300	400	500	650	250	300	400	500	650	250	300	400	500	650
A_1	0.71	0.77	0.88	0.57	0.68	0.82	1.31	0.92	1.04	2.96	1.04	1.13	1.40	1.05	0.97
$\phi_1(deg.)$	44.08	43.94	43.49	42.98	42.89	42.88	42.68	42.75	42.43	41.80	42.83	42.80	42.93	42.76	42.41
$E_{cp1}(eV)$	3.59	3.56	3.47	3.33	3.24	3.48	3.47	3.42	3.34	3.22	3.46	3.44	3.45	3.34	3.20
$\Gamma_1(eV)$	0.47	0.50	0.56	0.54	0.60	0.59	0.69	0.61	0.68	1.04	0.61	0.62	0.68	0.64	0.74
A_2	7.98	8.14	8.89	8.83	9.15	9.99	11.01	10.41	11.09	13.21	9.50	9.84	9.99	9.76	10.04
$\phi_2(deg.)$	40.14	40.13	40.09	39.92	39.93	40.00	40.02	39.96	39.86	39.80	40.11	40.10	40.11	40.03	39.92
$E_{cp2}(eV)$	4.39	4.37	4.30	4.21	4.13	4.32	4.30	4.26	4.20	4.13	4.29	4.26	4.25	4.20	4.13
$\Gamma_2(eV)$	0.79	0.81	0.84	0.83	0.87	0.71	0.75	0.75	0.79	0.86	0.78	0.80	0.82	0.83	0.88

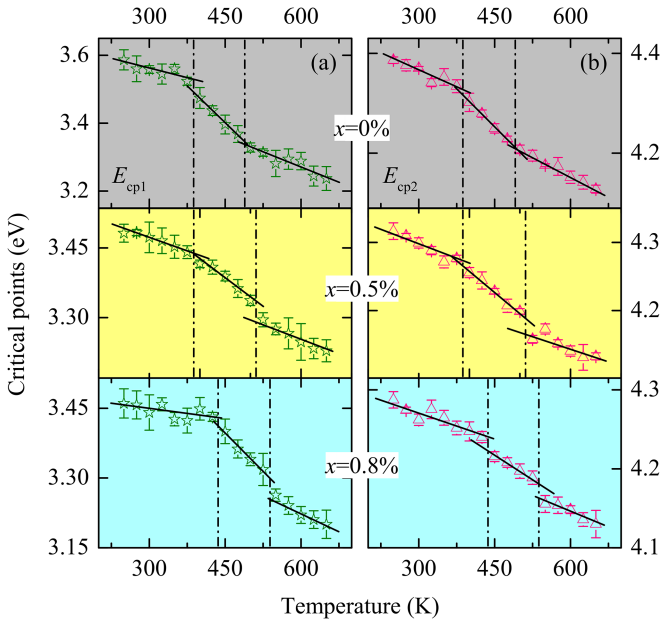

FIG. 2. Temperature dependence of two critical-point energies for (a) E_{cp1} and (b) E_{cp2} with linearly fitting results (solid lines). The dash-dot lines are applied to guide the eyes and indicate abnormity behavior.

the CPs of *x*%-Co:NBBT6 crystals can be approximately divided into three parts. To better identify the various trends of the CPs, every region was linearly fitted. It can be displayed that, interrupts of slope for E_{cp1} variation take place near 400 K for *x*=0% and 0.5%; 425 K for 0.8%. However, the deviations from linearity for E_{cp2} were merged near 500, 525, and 550 K for *x*=0%, 0.5%, and 0.8%, respectively.

To affirm the abnormal temperature-points of *x*%-Co:NBBT6 crystals observed from optical ellipsometry, Raman spectra were performed from 250 to 650 K, as displayed in Fig. 3(a). All measured Raman spectra have been corrected by the Bose-Einstein population factor, because the temperature dependence remaining after Bose-Einstein correction can only results from dynamical changes in the internal state of crystal system.[19] The assignment of normal-mode vibrations have been already discussed in previous work.[12] For all the three crystals, the scattering near 300 cm^{-1} shows an evidently red shift in frequency with increasing the temperature. In addition, the region of 400-650 cm^{-1} gradually appears as a single broadening band, due to the competition of intensity from three overlapping modes. These phenomena agree with the theory that higher structural disorder exists in the Ti-O bond and TiO_6 octahedra on heating.[11] Note that the scattering near 300 cm^{-1} is very sensitive to any structural transitions in perovskite ferroelectrics, which is related to vibrations of Ti-O bond, but also to the octahedron-tilt-related distortion bringing about important changes in this region.[5,14,19] To explore the effect of Co-doping on NBBT-6 single crystals, the modes involving Ti-O vibration are discussed by the means of both frequency and relative peak area ratio [Area($Ti-O_{mode}$)/Area($all-modes$)] against temperature, as shown in Fig. 3(b) and (c), respectively, which are obtained from well-fitted Lorentzian-shaped deconvolution. It's shown that, two visible discontinuities can be observed in both frequency shift and relative peak area ratio of Ti-O modes for all three samples, with every region fitted linearly. The first discontinuity appears near 400 K for *x*=0%, and 0.5%, 450 K for *x*=0.8%, respectively. While the second one exhibits at about 500, 525, and 550 K for *x*=0%, 0.5%, and 0.8%, respectively. These results accord with the observed discontinuous points from optical ellipsometry, which can point to structural variations. Notably, two abnormal temperatures have been reported from electrical experiments for Co modified NBBT*x*%-based system, which were identified as phase transition temperature of ferroelectric to anti-ferroelectric (T_{FE-AFE}), and anti-ferroelectric to paraelectric (T_{AFE-PE}).[6,8,20] In this work, the two abnormal temperatures, from optical ellipsometry and Raman results, are comparable to consequences from electrical experiments. Therefore, the two

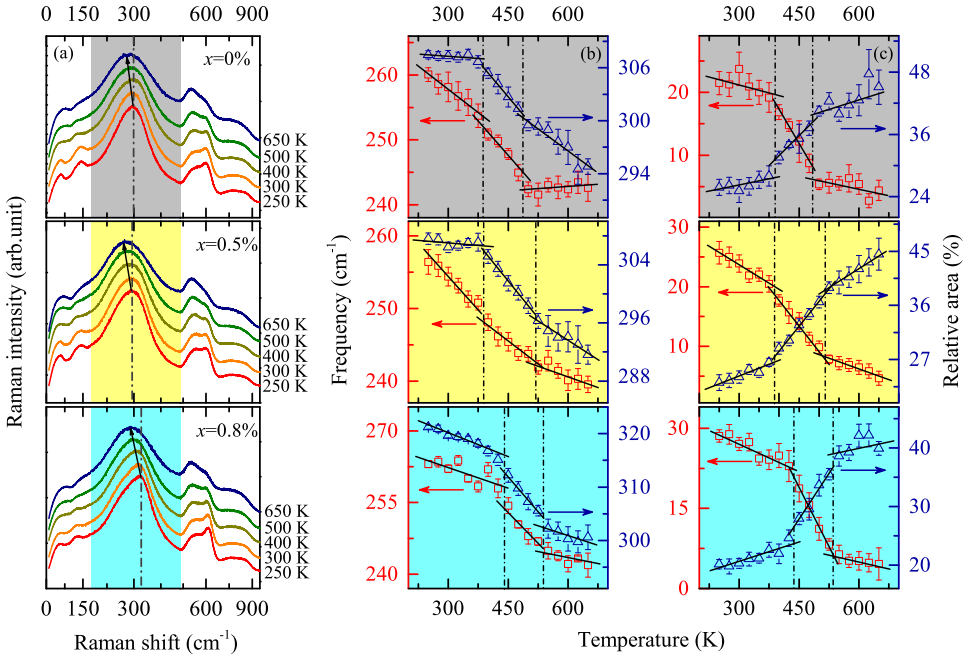

FIG. 3. (a) Temperature dependence Raman spectra of specimens from 250 to 650 K, with the arrows applied to guide the eyes. Note that all the spectra have been corrected by Bose-Einstein population factor to eliminate the effect of temperature on the peak intensities. Evolution of (b) frequency and (c) the relative area ratio of the Ti-O modes, with the symbol "□" and "△" corresponding to the left and right vertical axis, respectively. The phonon bands involving Ti-O vibration (colored parts) have been elongated and the dashed lines indicate the locations of the abnormal points.

abnormal temperatures of every x%-Co:NBBT6 crystals can be regarded as T_{FE-AFE} and T_{AFE-PE}, respectively. As can be seen, T_{FE-AFE} and T_{AFE-PE} exhibited an increasing trend with Co addition, indicating the restraining of phase transition.

Interestingly, abnormal phonon behaviors of x%-Co:NBBT6 crystals was observed when dealing with Raman spectra of x%-Co:NBBT6 crystals at the same temperature. Take the spectra at 300 K in Fig. 4(a) for example, with a total of 11 well-fitted Lorentzian-shaped deconvolution peaks. In comparison to the Raman spectra of pure NBBT-6, a slight shift towards lower frequency can be distinguished for x=0.5% near 300 cm^{-1} (related to modes involving Ti-O vibration). Whereas, for x=0.8%, the opposite shift is obviously observed for that region; In addition, peak near ~ 600 cm^{-1} also exhibits red shift. Furthermore, inset (b) depicts the prominent frequency variation of the modes near 300 cm^{-1} with the introduction of Co cations. It's worth noting that, the exact effect of dopant Co cations on phonon bands can be convincing with the spectral resolution in this work (better than 0.65 cm^{-1}).

Owing to the critical temperature-points (T_{FE-AFE} and T_{AFE-PE}) can be verified, it's credible to discuss the abnormal phonon behaviors of x%-Co:NBBT6 crystals for x=0.5% and 0.8%, which can be concerned with different relative ratio of Co^{2+} and Co^{3+} in the crystals. To clarify the valence state of Co cations in crystals, the X-ray Photoelectron spectra of Co $2p_{3/2}$ for x=0.5% and 0.8% were recorded in Fig. 5(a), which indicates asymmetric Co $2p_{3/2}$ band was partitioned into two sub-bands centered at 779.1 and 780.8 eV. Fig. 5(b) shows the relative atomic concentrations of Co^{2+}, which was derived from the fitting results of X-ray Photoelectron spectra. As can be discerned, the crystal with Co addition of 0.8 wt% has higher Co^{2+} concentration (36%) than that in 0.5 wt% (20%), which conforms the prediction for reverse phonon shift of modes related to Ti-O vibration in x=0.5% and 0.8%. Generally, dopant Co cations enter into the NBBT6 perovskite lattice to substitute B-site Ti^{4+} cations in the form of Co^{2+} or Co^{3+} states, because the radii of Co^{2+} (0.665 Å) or Co^{3+} (0.525 Å) are close to that of Ti^{4+} (0.605 Å).[21] In fact, it has been evidenced that Co-ion can stabilize in multiple valence states such as 2+ and 3+ in $Na_{0.5}Bi_{0.5}TiO_3$-based system, and their relative ratio depends on doping content.8 Furthermore, the coexistence of Co^{2+} and Co^{3+}

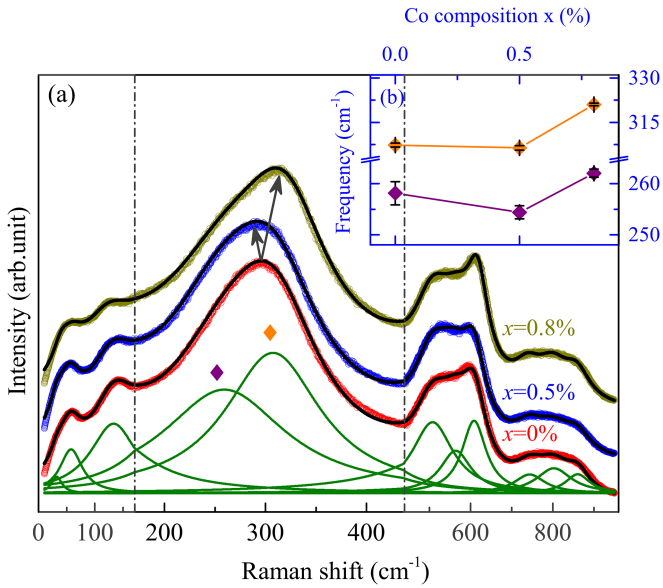

FIG. 4. (a) Raman spectra of x%-Co:NBBT6 (x=0%, 0.5%, and 0.8%) single crystals with different Co composition at 300 K. The green line stands for the Lorentzian-shaped spectral deconvolution of pure NBBT-6 single crystals. Note that phonon bands involving Ti-O vibration have been elongated, and arrows illustrate the variation trend of peak position. The inset (b) shows the frequency variation of the modes (♦) involving Ti-O vibration as a function of Co composition.

cations in NBBT6 crystal will affect the crystal lattice due to the difference in valence and radius. In fact, Co ions substituting for Ti^{4+} will generate the oxygen vacancies in the lattice, which will shrink the unit cell.[6,8] Note that, it is the clamping effect of oxygen vacancies on domain walls that restrain ferroelectric to anti-ferroelectric and anti-ferroelectric to paraelectric phase transition with Co addition. Besides, the incorporation of smaller radius Co^{3+} cations (0.525 Å) in the B-site sublattice of the ABO_3 perovskite is also helpful for the reduction in unit cell volume.[8] That is to say, the substitution by Co^{3+} results in the red shift of the modes involving Ti-O vibration in Raman spectra.[5,11] Whereas, the incorporation of larger radius Co^{2+} cations (0.605 Å) leads to an expansion of the unit cells, which can offset the lattice shrinkage induced by oxygen vacancies and benefits the displacement of Ti^{4+}. In other words, the substitution by Co^{2+} makes an opposite effect in frequency shift, i.e., bule shift. Therefore, it can be concluded that reverse phonon shift of the modes related to Ti-O vibration is ascribed to different relative concentration of Co^{2+} and Co^{3+} in the crystals of x=0.5% and x=0.8%.

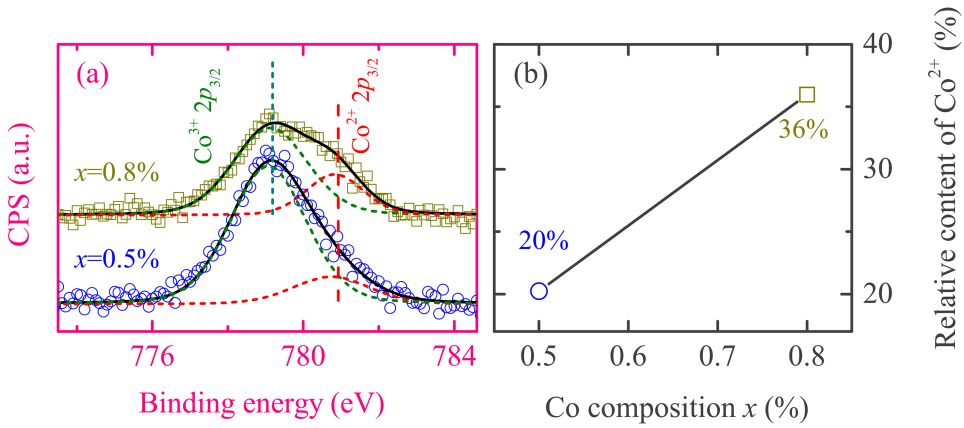

FIG. 5. (a) XPS spectra of Co $2p_{3/2}$ and (b) the dependence of relative content of Co^{2+} in the crystals for x=0.5% and 0.8%.

IV. SUMMARY

In summary, optical properties, electronic structures, and structural variations of x%-Co:NBBT6 (x=0%, 0.5% and 0.8%) single crystals have been investigated by optical ellipsometry and Raman spectra as a function of temperature from 250 to 650 K, respectively. Two critical temperature-points were found based on analysis of electronic transition and phonon modes, which are related to ferroelectric, anti-ferroelectric and paraelectric transitions, and exhibit an increasing trend with Co dopants. Furthermore, abnormal phonon behaviors in the crystal of x=0.5% and 0.8% were observed from Raman spectra, showing reverse frequency shift of the modes involving Ti-O vibration. It can be ascribed to different relative concentration of Co^{2+} and Co^{3+} in x=0.5% and x=0.8%, as confirmed by X-ray Photoelectron spectra data.

ACKNOWLEDGMENTS

This work was financially supported by Major State Basic Research Development Program of China (Grant No. 2013CB922300), Natural Science Foundation of China (Grant Nos. 11374097, 61376129, and 61504156), Projects of Science and Technology Commission of Shanghai Municipality (Grant Nos. 15JC1402100 and 14XD1401500), and the Program for Professor of Special Appointment (Eastern Scholar) at Shanghai Institutions of Higher Learning.

[1] T. Takenaka, K. Maruyama, and K. Sakata, Jpn. J. Appl. Phys. **30**, 2236 (1991).
[2] W. W. Ge, C. T. Luo, Q. H. Zhang, Y. Ren, J. F. Li, H. S. Luo, and D. Viehland, Appl. Phys. Lett. **105**, 162913 (2014).
[3] C. Chen, X. Jiang, Y. Li, F. Wang, Q. Zhang, and H. Luo, J. Appl. Phys. **108**, 124106 (2010).
[4] T. Huang, Z. G. Hu, G. S. Xu, X. L. Zhang, J. Z. Zhang, and J. H. Chu, Appl. Phys. Lett. **104**, 111908 (2014).
[5] D. Schütz, M. Deluca, W. Krauss, A. Feteira, T. Jackson, and K. Reichmann, Adv. Funct. Mater. **22**, 2285 (2012).
[6] Q. Xu, M. Chen, W. Chen, H.-X. Liu, B.-H. Kim, and B.-K. Ahn, Acta Mater. **56**, 642 (2008).
[7] H.-D. Li, C.-D. Feng, and W.-L. Yao, Mater. Lett. **58**, 1194 (2004).
[8] H. C. Hu, M. K. Zhu, F. Y. Xie, N. Lei, J. Chen, Y. D. Hou, and H. D. Yan, J. Am. Ceram. Soc. **92**, 2039 (2009).
[9] M.-P. Zheng, Y.-D. Hou, F.-Y. Xie, J. Chen, M.-K. Zhu, and H. Yan, Acta Mater. **61**, 1489 (2013).
[10] G.-Z. Zang, X.-J. Yi, J. Du, and Y.-F. Wang, Mater. Lett. **64**, 1394 (2010).
[11] M. Zannen, H. Khemakhem, A. Kabadou, and M. Es-Souni, J. Alloys Compd. **555**, 56 (2013).
[12] T. Huang, S. Guo, L. P. Xu, C. Chen, H. S. Luo, J. H. Chu, and Z. G. Hu, J. Appl. Phys. **117**, 224103 (2015).
[13] X. J. Ding, L. P. Xu, Z. G. Hu, X. F. Chen, G. S. Wang, X. L. Dong, and J. H. Chu, Appl. Phys. Lett. **105**, 131909 (2014).
[14] S. Trujillo, J. Kreisel, Q. Jiang, J. H. Smith, P. A. Thomas, P. Bouvier, and F. Weiss, J. Phys.: Condens. Matter **17**, 6587 (2005).
[15] X. Chen, Z. G. Hu, Z. H. Duan, X. F. Chen, G. S. Wang, X. L. Dong, and J. H. Chu, J. Appl. Phys. **114**, 043507 (2013).
[16] M. Zeng, S. W. Or, and H. L. W. Chan, J. Appl. Phys. **107**, 043513 (2010).
[17] H. Y. Tian, W. G. Luo, X. H. Pu, X. Y. He, P. S. Qiu, A. L. Ding, S. H. Yang, and D. Mo, J. Phys.: Condens. Matter **13**, 4065 (2001).
[18] A. Bouaine, N. Brihi, G. Schmerber, C. Ulhaq-Bouillet, S. Colis, and A. Dinia, J. Phys. Chem. C **111**, 2924 (2007).
[19] K. Datta, A. Richter, M. Göbbels, R. B. Neder, and B. Mihailova, Phys. Rev. B **90**, 064112 (2014).
[20] K. Thangavelu, R. Ramadurai, and S. Asthana, AIP Advances **4**, 017111 (2014).
[21] R. D. Shannon and C. T. Prewitt, Acta Crystallogr., Sect. B **25**, 925 (1969).